Hydrology and Earth System Sciences

Open Access

Discussions

Technical Note: The use of an interrupted-flow centrifugation method to characterise preferential flow in low permeability media

R. A. Crane[1,2], M. O. Cuthbert[2,3], and W. Timms[2,4]

[1]School of Civil and Environmental Engineering, UNSW, Sydney, Australia
[2]Connected Waters Initiative Research Centre, UNSW, Sydney, Australia
[3]School of Geography, Earth and Environmental Sciences, University of Birmingham, UK
[4]School of Mining Engineering, UNSW, Sydney, Australia

Correspondence to: R. A. Crane (r.crane@unsw.edu.au)

Abstract

We present an interrupted-flow centrifugation technique to characterise preferential flow in low permeability media. The method entails a minimum of three phases: centrifuge induced flow, no flow and centrifuge induced flow, which may be repeated several times in order to most effectively characterise multi-rate mass transfer behaviour. In addition, the method enables accurate simulation of relevant in situ total stress conditions during flow by selecting an appropriate centrifugal force level. We demonstrate the utility of the technique for characterising the hydraulic properties of smectite clay dominated core samples. All samples exhibited a non-Fickian tracer breakthrough (early tracer arrival), combined with a decrease in tracer concentration immediately after each period of interrupted-flow. This is indicative of dual (or multi) porosity behaviour, with solute migration predominately via advection during induced flow, and via molecular diffusion (between the preferential flow network(s) and the low hydraulic conductivity domain) during interrupted-flow. Tracer breakthrough curves were simulated using a bespoke dual porosity model with excellent agreement between the data and model output (Nash–Sutcliffe model efficiency coefficient was > 0.97 for all samples). In combination interrupted-flow centrifuge experiments and dual porosity transport modelling are shown to be a powerful method to characterise preferential flow in low permeability media.

1 Introduction

It is well known that heterogeneities, including biogenic pores/channels, desiccation cracks, fissures, fractures, non-uniform particle size distributions and inter-aggregate pores, are widespread in the subsurface and lead to a range of preferential flow phenomena (Beven and Germann, 1982; Cuthbert et al., 2013; Cuthbert and Tindimugaya, 2010; Flury et al., 1994). The coexistence of relatively high hydraulic conductivity (K) domain(s) and an impermeable one, often termed dual porosity, results in a non-

Fickian breakthrough curve. Solute transport in such systems is often characterised by an early arrival of solutes originating from the more mobile domain (macropores) and a slow approach to the final concentration caused by diffusion into the immobile domain (matrix or microporous network). When fitting breakthrough curves, therefore,

5 it is often difficult to differentiate between contributions from the micro- and macropore transport mechanisms. As a consequence, in recent years there has been much research into the development of effective empirical and modelling techniques to characterise solute transport processes for dual porosity systems. One method investigated has been the use of interrupted-flow solute break-through experiments. Amongst the

10 original work on this topic Murali and Aylmore (1980) discussed the influence of non-constant flow on solute transport in aggregated soil. Brusseau et al. (1989) developed a flow-interruption method for use in measuring rate-controlled sorption processes in soil systems, which was subsequently applied by Koch and Fluhler (1993) to investigate advection and diffusion phenomena occurring for nonreactive solute transport in

15 aggregated media. The idea proposed was that by interrupting flow during nonreactive tracer breakthrough the degree of non-equilibrium between any fast and slow flow pathways can be determined. Central to this hypothesis is that the magnitude of the change in nonreactive tracer concentration in effluent samples taken immediately after a no-flow period is indicative of such non-equilibrium. Subsequent work within this field

20 has included: determination of physical (e.g. diffusive mass transfer between advective and nonadvective water) and chemical (e.g. nonlinear sorption) nonequilibrium processes in soil (Brusseau et al., 1997); determination of nonreactive solute exchange between the matrix porosity and preferential flow paths in fractured shale (Reedy et al., 1996); quantifying the effect of aggregate radius on diffusive timescales in dual porosity

25 media (Cote et al., 1999); numerical modelling of aqueous contaminant release in non-equilibrium flow conditions (Wehrer and Totsche, 2003); empirical modelling of the release of dissolved organic species (Guimont et al., 2005; Ma and Selim, 1996; Totsche et al., 2006; Wehrer and Totsche, 2005, 2009) and heavy metals (Buczko et al., 2004); increasing the efficiency of solute leaching (Cote et al., 2000); empirical modelling of

conservative tracer transport in a laminated sandstone core sample (Bashar and Tellam, 2006); and characterising in situ aquifer heterogeneity (Gong et al., 2010). One area where comparatively few studies exist, however, is in characterising the hydraulic properties of aquitards (e.g. clay dominated soils and sediments, shales, mudstones),

5 which may have preferential flow paths which compromise their integrity as barriers to the movement of groundwater contaminants. There are, presently, significant technical difficulties in characterising such features at appropriate scales (Cuthbert et al., 2010). For example, it is well known that the hydraulic conductivity of glacial till is scale dependent, with laboratory permeability measurements yielding values orders of mag-

10 nitude lower than field based measurements and modelling (Cuthbert et al., 2010). As a consequence a key requirement of laboratory scale aquitard characterisation is that the core sample must be of sufficient volume in order to incorporate the key dual porosity features which govern the overall formation. A second technical challenge is that laboratory testing typically requires generation of flow through the sample whilst

15 maintaining relevant in situ hydro-geotechnical conditions. One method which has been demonstrated as effective for this purpose is centrifugation, which is increasingly being used for hydraulic and geotechnical testing of low K materials (Hensley and Schofield, 1991; Nimmo and Mello, 1991; Timms et al., 2009; Timms and Hendry, 2008). Moreover, experiments using geotechnical centrifuges with payload capacities exceeding

20 several kilograms can provide the additional benefit of being able to use core samples of representative scale for the overall formation. Here we present, for the first time, an interrupted-flow methodology using a centrifuge permeameter (CP) to characterise dual porosity behaviour of low permeability porous media. A novel dual domain model is also described which has been used to guide physical interpretation of the experi-

25 mental tracer breakthrough curves.

Technical Note: The use of an interrupted-flow centrifugation method

R. A. Crane et al.

2 Experimental methods

2.1 Core and groundwater sampling methodology

The clay core (101.6 mm in diameter, Treifus core barrel, non-standard C size) and groundwater were sourced from a 40 m thick, semi-consolidated, clay-rich alluvium deposit located approximately 100 km south of Gunnedah, New South Wales, Australia (31°31′9″ S, 150°28′7″ E). Equipment and procedures for obtaining minimally disturbed cores were compliant with ASTM 2012. See Timms et al. (2014) for a review of the procedure. Groundwater samples were taken from piezometers using standard groundwater quality sampling techniques (Sundaram et al., 2009). A 240V electric submersible pump (GRUNDFOS MP1) and a surface flow cell were used to obtain representative samples after purging stagnant water to achieve constant field measurements of EC, pH, dissolved oxygen (DO) and Eh.

2.2 Centrifuge permeameter theory

During centrifugation increased centrifugal force generates a body force which accelerates both solid and fluid phases within the sample. Centrifugal acceleration at any point within a centrifuge sample is calculated as follows:

$$a = \omega^2 r \qquad (1)$$

where a is the centrifugal acceleration ($m\,s^{-2}$), ω is the angular velocity ($radians^{-1}$), and r is the radius from the axis of rotation (m). The g level is the scaling factor (a/g) for accelerated gravity, where g is gravity at earth's surface.

K ($m\,s^{-1}$) is calculated using ASTM (2000) (Eq. 2), where: Q = the steady-state fluid flux ($mL\,h^{-1}$); A = the sample flow area (cm^2); r_m = the radial distance at the mid-point of the core sample (cm); and RPM = revolutions per minute.

$$K = \frac{0.248Q}{Ar_\mathrm{m}(\mathrm{RPM})^2} \tag{2}$$

The estimated in situ stress applied at the base of the core samples was calculated according to Eq. (3), and assumes that the overlaying formations were fully saturated and of a similar density to the core samples.

5 $$\sigma_\mathrm{i} = \rho_\mathrm{s}dg \tag{3}$$

where σ_i = in situ stress (kPa); ρ_s = saturated density of core (kg m^{-3}); d = depth to the base of the core sample (m BGL); and g = gravitational acceleration (m s^{-2}). The applied stress at the base of the core (σ_g, kPa) during the centrifuge experiments was calculated according to Eq. (4) (Timms et al., 2014).

10 $$\sigma_g = [(\rho_\mathrm{b}L_\mathrm{c}) + \rho_\mathrm{w}(L_\mathrm{c} + h_\mathrm{w})]a_\mathrm{b} \tag{4}$$

where ρ_b = core bulk density (kg m^{-3}); L_c = length of CP core specimen (mm); ρ_w = influent density (kg m^{-3}); h_w = height of influent water above CP core specimen (mm); and a_b is the centrifugal acceleration at the base of the CP core specimen.

2.3 Centrifuge permeameter sample preparation

15 A Broadbent geotechnical centrifuge (GMT GT 18/0.7 F) with a custom built permeameter module (Timms et al., 2014) was used for this study. Prior to mounting into the CP the outer 5 mm of the clay cores were trimmed and inserted into Teflon cylindrical core holders (100 mm internal diameter, 220 mm length) using a custom built mechanical cutting and loading device. A 5 mm thick A14 Geofabrics Bidim geofabric filter (100 micron, $K = 33$ m s^{-1}) was placed above and below the sample in order to prevent clogging of the effluent drainage plate with colloid material from the sample. The geofabric filter was held in position above the sample using a plastic clamp.

The core holders (with the core sample held within) were placed into 3000 mL glass beakers containing 1000 mL of groundwater derived from the piezometer at the closest depth to the core sample (see Table 1) and allowed to saturate from the base upwards. This was performed by immersing the core holder into a reservoir of groundwater with the level of the water 5 cm higher than the top of the core sample. The mass of each core was then monitored every 24 h until no further increase in mass was recorded, saturation was then assumed to have occurred. The core holders (containing the saturated core samples) were mounted to the CP system via double O-ring seals. An influent head was added to all samples (see Table 1), which was maintained during centrifugation by a custom built automated influent level monitoring and pumping system. The system comprises of a carbon fibre EC electrode array which is connected via a fibre optic rotary joint to a peristaltic pump that supplies influent from an external 100 mL burette. Effluent samples were collected in an effluent reservoir and extracted using a 50 mL syringe. All experiments were conducted under steady-state flow, which is defined as a < 10 % difference between influent and effluent flow rates. The influent volume was determined by manual measurements of the water level in the external burette and effluent volumes were measured by multiplying their mass by their density.

2.4 Interrupted-flow experiment methodology

The idea of interrupting the flow during a breakthrough experiment is to differentiate between advection and diffusion processes. The method comprises a minimum of three phases:

1. Flow is induced at a constant centrifugal force for a fixed time period with effluent samples collected at multiple periodic intervals. The g level and influent reservoir height are selected so that the maximum total stress on the core approached the estimated in situ stress of the material at the given depth in the formation (Eqs. 3 and 4). The time period between each effluent sampling interval is selected in

order to gain sufficient effluent volume (namely > 1 mL) for accurate volume and nonreactive tracer concentration measurement.

2. Flow is interrupted (stopped) for a fixed time period during which time the permeameters are disconnected from the centrifuge module and positioned upright, the influent reservoir is also removed to limit any downward migration of solutes. A relatively long interrupted-flow period (> 12 h) is selected so that slow mass transfer processes can be identified.

3. Phase 1 is then repeated.

All phases can be repeated multiple times in order to record sufficient non-reactive tracer breakthrough which enables the mass transport behaviour to be accurately characterised. Deuterium oxide (D_2O) (Acros Organics, 99.8 % concentration) was used as a non-reactive tracer. A concentration of $3.12\,\mathrm{mL\,L^{-1}}$ was used, which raised the concentration of D_2O to approximately 200 %. This was selected as sufficiently high in order to result in accurately measureable mass transfer changes. Effluent samples were filtered using a 0.2 μm cellulose acetate filter, stored at 4 °C and analysed for δD within 7 days of testing. δD was determined by measuring the $^1H/^2H$ ratio to an accuracy of 0.1 % using a Los Gatos DLT100 isotope analyser.

2.5 Dual domain transport modelling

Dual porosity models were created using COMSOL Multiphysics (v. 4.4) modified from well-known formulations described, for example, by Coats and Smith (1964), Bear (1987) and Gerke and van Genuchten (1993). The purpose of the modelling was to aid physical interpretation of the tracer breakthrough curves and validate the hypothesis that the step changes in tracer concentrations observed during no-flow periods could be explained by the presence of dual porosity in the samples. The models comprised a classical advection-dispersion equation for a mobile zone (subscript m) representing preferential flow pathways with a source/sink term representing exchange of solute with

an immobile zone (subscript im). Solute transport in the immobile zone was by diffusion only. The exchange flux between the immobile and mobile zones was modelled as being proportional to the concentration difference between the zones. The governing equations are as follows:

$$\frac{\partial C_m}{\partial t} = D_m \frac{\partial^2 C_m}{\partial z^2} - \frac{q(t)}{\varnothing_m} \frac{\partial C_m}{\partial z} - \frac{\gamma}{\varnothing_m}(C_m - C_{im}) \tag{5}$$

$$\frac{\partial C_{im}}{\partial t} = \mu \frac{\partial^2 C_{im}}{\partial z^2} + \frac{\gamma}{\varnothing_{im}}(C_m - C_{im}) \tag{6}$$

$$D_m = \frac{\propto q(t)}{\varnothing_m} + \mu \tag{7}$$

where C is the δD isotope ratio [1], t is time [T], z is distance along the column [L], q is fluid flux [LT^{-1}], α is hydrodynamic dispersivity [L], μ is the coefficient of molecular diffusion [L^{2}T^{-1}]. The porosity, $\varnothing$, of the mobile and immobile domain is defined as:

$$\varnothing_m = \frac{V_{p,m}}{V_T} \tag{8}$$

$$\varnothing_{im} = \frac{V_{p,im}}{V_T} \tag{9}$$

where $V_{p,m}$ is the pore volume of the mobile domain [L], $V_{p,im}$ is the pore volume of the immobile domain [L] and V_T is the total volume of the saturated core [L]. The mass transfer coefficient, γ [T^{-1}], is defined as:

$$\gamma = \frac{\beta \varnothing_m \mu}{a^2} \tag{10}$$

where β is the dimensionless geometry coefficient, which typically ranges from 3 for rectangular slabs to 15 for spherical aggregates, and a is the characteristic half width of the matrix block [L] (Gerke and van Genuchten, 1993).

75

Variable flux boundary conditions were used for both flow and transport into the mobile domain and q varied according to the measured flow rate during each effluent sampling interval. A novel aspect to the models, facilitated by the flexibility of model structure variations possible in COMSOL, was that the upstream transport boundary for the immobile zone was defined using a Dirichlet (constant concentration) condition during times of centrifugation, but switched to a no-flow condition during the interrupted-flow phases. The downstream transport boundary flux was set equal to the sum of the advective and diffusive flux components at a large distance downstream to ensure the results at the column outlet distance were not sensitive to its position. The total mass flux at the distance from the upstream boundary corresponding with the length of the experimental column was output from the models and integrated over the sampling periods for comparisons to the observed breakthrough curves. μ was calculated as $3.43 \times 10^{-5}\,\mathrm{m^2\,d^{-1}}$ which is the diffusion coefficient of D_2O in H_2O at $25.0\,°C$ (Orr and Butler, 1935) multiplied by the average tortuosity of 0.15 reported by Barnes and Allison (1988) for clay bearing media. Model output was fitted to the observed data by varying the unconstrained parameters: α and γ. Note that $\varnothing_m$ and $\varnothing_{im}$ were also considered unconstrained parameters, but their sum was constrained to equal the $\varnothing_T$ measured for each sample by oven drying at $105\,°C$ for $24\,h$. In order to quantify the deviation between the recorded data and the dual porosity model the normalised root-mean-square error (NRMSE) and the Nash–Sutcliffe model efficiency coefficient (NSMEC) were calculated (Nash and Sutcliffe, 1970). The mesh size and model tolerance were set sufficiently small so that the results were no longer sensitive to further reduction to ensure the accuracy of the model output. The models runs presented were all executed using an extra fine mesh size and a relative tolerance of 0.00001.

2.6 Dual domain model sensitivity testing

Sensitivity analysis of the dual domain model (for the core taken from $5.03\,\mathrm{m}$) was conducted in order to determine how sensitive the model was to changes in the constrained (L, $\varnothing$ and μ) and unconstrained ($\varnothing_m$, α and γ) parameters. Sensitivity factors

for constrained parameters were determined according to the estimated percentage error associated with each parameter, whilst ±50 % was selected for the unconstrained parameters in order to determine their influence on the NSMEC. The percentage error for L was calculated to be ±2.78 % due to the core length being 36 mm and the error associated with measurement at each end was ± 0.5 mm. The percentage error for ⌀ was calculated to be ±2.79 % which comprises the L measurement error plus 0.0026 % which is the calculated error associated with the two mass measurements. The percentage error for μ was determined to be ±50 % due to the range in tortuosity of 0.1–0.2 documented by Barnes and Allison (1988) and references therein.

3   Results and discussion

3.1   D₂O breakthrough

D_2O breakthrough data and best fit dual porosity model output for the interrupted-flow experiments conducted using core samples taken from 5.03, 9.52 and 21.75 m depth BGL are displayed in Fig. 1. A close fit was achieved between the dual porosity model output and the original data, with a NSMEC of 0.97, 0.99 and 0.97 recorded for D_2O breakthrough data from core samples taken from 5.03, 9.52 and 21.75 m depth BGL respectively. The D_2O breakthrough curves for all core samples exhibited a relatively elongated shape, with 100 % breakthrough not recorded for any of the timescales tested. This was expected given that a "long tailing" is a common feature of dual (or multi) porosity materials, i.e. systems where the mobile domain is coupled to a less mobile, or immobile, domain. In such instances the dominant solute transport mechanism during imposed flow in the mobile domain(s) is typically advection, however, solute exchange also occurs in parallel with the immobile domain(s), typically via molecular diffusion. Following each interrupted-flow (no flow) period a decrease in δD was recorded for all samples, and attributed to the diffusion of D_2O from the preferential flow domain(s) into the low-flow (or immobile) flow domain(s). The shape of the D_2O break-

through curves and the magnitude of the δD decrease following the interrupted-flow periods are different for all samples, with a 42.6, 18.5 and 28.4 % decrease recorded for the core samples taken from 5.03, 9.52 and 21.75 m depth BGL respectively after the first interrupted-flow period. In addition, the K_v of each sample was recorded as different ent (Fig. 2), with average values of $1.4{\times}10^{-8}\,\mathrm{m\,s^{-1}}$, $3.9{\times}10^{-9}\,\mathrm{m\,s^{-1}}$ and $2.7{\times}10^{-9}\,\mathrm{m\,s^{-1}}$ for the core samples taken from 5.03, 9.52 and 21.75 m depth BGL respectively. The K_v was recorded to decrease during the initial stages of each centrifugation period, and attributed to the partial consolidation of the clay due to the stress applied by the centrifugal force. Following this initial consolidation period a more constant K_v as a function of time was recorded for all cores, indicating that relative equilibrium had been achieved between stress applied by the centrifugal force and the compaction state of the core.

3.2 Dual domain model

The close model fits confirm that preferential flow through a dual porosity structure is a plausible hypothesis to explain the shape of the observed breakthrough curves. The unconstrained ($\varnothing_m$, α and γ) parameters that yielded the best dual domain model output fit to the D_2O breakthrough data are displayed in Table 2. It is noted that the pore volume of the mobile domain per total volume of the core, $\varnothing_m$, was modelled to be 0.04, 0.04 and 0.08 for core taken from 5.03, 9.52 and 21.75 m depth BGL respectively. With total porosity, $\varnothing$, measured as 0.44, 0.47 and 0.43 this equates to 9.1, 8.5 and 18.6 % of the total pore volume respectively, suggesting that preferential flow features comprise a relatively large proportion of the total pore porosity in each sample. Hydrodynamic dispersivity, α, for best fit model output for all core samples was $L/2$, which is larger than typically reported for laboratory scale column experiments (e.g. Shukla et al., 2003). It can be noted that all of the core samples were assumed to have remained saturated throughout the breakthrough experiments because all influent and effluent flow rates were recorded at steady-state. Whilst dispersion is known to increase substantially as moisture content decreases from saturation (e.g. Wilson and Gelhar, 1981) it is therefore unlikely that this could have been a factor. The mass transfer co-

efficient, γ, was also modelled as different for each core sample with 0.65, 1.50 and 1.20 yielding the best model fit for the core samples taken from 5.03, 9.52 and 21.75 m depth BGL respectively. Using Eq. (10) the half width of the matrix block (using $\beta = 15$ for an idealised parallel fracture geometry after Gerke and van Genuchten, 1993), a, is calculated as 17.8, 12.1 and 12.3 mm for the core samples taken from 5.03, 9.52 and 21.75 m depth BGL respectively. This suggests that the preferential flow channels present are likely to be separated by distances in the order of several mm from each other within the cores. With the dimensions of the cores significantly greater than these values the model output therefore suggests that several preferential flow features are present in each core sample.

Model output for the mobile and immobile domains at the top, middle and base of the core samples is displayed in Fig. 3. It is noted that for all core samples diffusion into the immobile domain during the induced flow periods is relatively significant, with $\delta D_{im}/\delta D_m$ at the end of the first centrifugation (induced flow) period recorded as 0.16, 0.32 and 0.34 for the base of the core samples taken from 5.03, 9.52 and 21.75 m depth BGL respectively. With respective average flow rates recorded as 0.017, 0.007 and 0.015 m d^{-1} this behaviour is not obviously related to the variation in flow rates between the samples, but more likely to the intrinsic properties of the preferential flow domain (namely: $\varnothing_m$, γ and α). It is also noted that for all core samples full equilibration between the mobile and immobile domains occurred ($\delta D_{im} = \delta D_m$) during each no flow period. For example, δD_{im} and δD_m were modelled to be within ±1 % of each other after 7.0, 2.6 and 6.1 h during the first no flow period for the core samples taken from 5.03, 9.52 and 21.75 m depth BGL respectively.

3.3 Sensitivity analysis

Sensitivity analysis plots for a ±50 % change in unconstrained parameters (α, γ and $\varnothing_m$) for the core sample taken from 5.03 m depth BGL are displayed in Fig. 4, with corresponding NSMEC data displayed in Table 3. The model fitting efficiency is relatively insensitive to all three unconstrained parameters in the range tested, with a less than

12 % change in the NSMEC compared to the NSMEC recorded for the best fit (Table 3). Sensitivity for the estimated % error associated with constrained parameters ($\varnothing$, L and μ) are displayed in Fig. 5, with corresponding NSMEC data displayed in Table 3. The model fitting efficiency is also relatively insensitive, with a less than 1 % change in the NSMEC compared to the NSMEC recorded for the best fit (Table 3).

4 Conclusions and outlook

Solute transport in the subsurface can be influenced by multiple nonlinear, rate-limited processes, and it is often difficult to determine which processes predominate for any given system. In this work we demonstrate the utility of interrupted-flow solute transport experiments using a CP to quantify the relative contributions of preferential flow pathways and surrounding matrix porosity to mass transfer processes in low permeability dual porosity materials. Dual domain transport modelling was used to validate the hypothesis that the step changes in tracer concentrations observed during no-flow periods could be explained by the presence of dual porosity in the samples. The modelling also enabled aspects of the physical properties of the two domains to be inferred. Smectite clay core samples were used (101.6 mm in diameter) as an example low K dual porosity media, however, it is anticipated that the methodology would also be suitable for the characterisation of any dual porosity material where mass transfer occurs via both advection and diffusion (e.g. fractured rock, heterogeneous soils, mine tailings). The methodology entails a minimum of three phases: induced flow, no flow, and induced flow, however, this may be repeated several times in order to most effectively characterise the multi-rate mass transfer behaviour. In addition, it is necessary to tailor the induced flow rate, interrupted-flow timescales and non-reactive tracer concentrations in order to most effectively identify different mass transfer processes whilst also simulating realistic total stress conditions. Future work will seek to further investigate the structure of the clay samples studied using quantitative tomography techniques

(e.g. X-ray computed tomography and magnetic resonance imaging) and how these physical features can be integrated into site scale numerical flow modelling.

References

ASTM: Standard test method for determining unsaturated andsaturated hydraulic conductivity in porous media by steady-state centrifugation, ASTM D6527, West Conshohoken, PA, 2000.

ASTM: Standard practice for thin-walled tube sampling of soils for geotechnical purposes, ASTM D1587-08(2012)e1, West Conshohocken, PA, 2012.

Barnes, C. J. and Allison, G. B.: Tracing of water movement in the unsaturated zone using stable isotopes of hydrogen and oxygen, J. Hydrol., 100, 143–176, 1988.

Bashar, K. and Tellam, J. H.: Non-reactive solute movement through saturated laboratory samples of undisturbed stratified sandstone, Geol. Soc. Sp., 263, 233–251, 2006.

Bear, J. and Bachmat, Y.: Introduction to Modeling of Transport Phenomena in Porous Media, Kluwer Academic Publishers, Dordrecht, Boston, London, 553 pp., 1990.

Beven, K. and Germann, P.: Macropores and water flow in soils, Water Resour. Res., 18, 1311–1325, 1982.

Brusseau, M. L., Rao, P. S. C., Jessup, R. E., and Davidson, J. M.: Flow interruption: a method for investigating sorption nonequilibrium, J. Contam. Hydrol., 4, 223–240, 1989.

Brusseau, M. L., Hu, Q., and Srivastavaa, R.: Using flow interruption to identify factors causing nonideal contaminant transport, J. Contam. Hydrol., 24, 205–219, 1997.

Title Page

Abstract | Introduction

Conclusions | References

Tables | Figures

◄◄ | ►►

◄ | ►

Back | Close

Full Screen / Esc

Printer-friendly Version

Interactive Discussion

Buczko, U., Hopp, L., Berger, W., Durner, W., Peiffer, S., and Scheithauer, M.: Simulation of chromium transport in the unsaturated zone for predicting contaminant entries into the groundwater, J. Plant Nutr. Soil Sc., 167, 284–292, 2004.

Coats, K. H. and Smith, B. D.: Dead-end pore volume and dispersion in porous media, Soc. Pet. Eng. J., 4, 73–84, 1964.

Cote, C. M., Bristow, K. L., and Ross, P. J.: Quantifying the influence of intra-aggregate concentration gradients on solute transport, Soil Sci. Soc. Am. J., 63, 757–767, 1999.

Cote, C. M., Bristow, K. L., and Ross, P. J.: Increasing the efficiency of solute leaching: impacts of flow interruption with drainage of the "preferential flow paths", J. Contam. Hydrol., 43, 191–209, 2000.

Cuthbert, M. O. and Tindimugaya, C.: The importance of preferential flow in controlling groundwater recharge in tropical Africa and implications for modelling the impact of climate change on groundwater resources, J. Water Clim. Change, 1, 234–245, 2010.

Cuthbert, M. O., Mackay, R., Tellam, J. H., and Thatcher, K. E.: Combining unsaturated and saturated hydraulic observations to understand and estimate groundwater recharge through glacial till, J. Hydrol., 391, 263–276, 2010.

Cuthbert, M. O., Mackay, R., and Nimmo, J. R.: Linking soil moisture balance and source-responsive models to estimate diffuse and preferential components of groundwater recharge, Hydrol. Earth Syst. Sci., 17, 1003–1019, doi:10.5194/hess-17-1003-2013, 2013.

Flury, M., Fluhler, H., Jury, W. A., and Leuenberger, J.: Susceptibility of soils to preferential flow of water: afield study, Water Resour. Res., 30, 1945–1954, 1994.

Gerke, H. H. and van Genuchten, M. T.: Evaluation of a first-order water transfer term for variably saturated dual-porosity flow models, Water Resour. Res., 29, 1225–1238, 1993.

Gong, R., Lu, C., Wu, W.-M., Cheng, H., Gu, B., Watson, D. B., Criddle, C. S., Kitanidis, P. K., Brooks, S. C., Jardine, P. M., and Luo, J.: Estimating kinetic mass transfer by resting-period measurements in flow-interruption tracer tests, J. Contam. Hydrol., 117, 37–45, 2010.

Guimont, S., Perrin-ganier, C., Real, B., and Schiavon, M.: Effects of soil moisture and treatment volume on bentazon mobility in soil, Agron. Sustain. Dev., 25, 323–329, 2005.

Hensley, P. J. and Schofield, A. N.: Accelerated physical modelling of hazardous-waste transport, Geotechnique, 41, 447–465, 1991.

Koch, S. and Fluhler, H.: Non-reactive solute transport with micropore diffusion in aggregated porous media determined by a flow-interruption method, J. Contam. Hydrol., 14, 39–54, 1993.

Technical Note: The use of an interrupted-flow centrifugation method

R. A. Crane et al.

Title Page

Abstract	Introduction
Conclusions	References
Tables	Figures

◄◄ ►►

◄ ►

Back Close

Full Screen / Esc

Printer-friendly Version

Interactive Discussion

Ma, L. and Selim, H. M.: Solute transport in soils under conditions of variable flow velocities, Water Resour. Res., 32, 3277–3283, 1996.

Murali, V. and Aylmore, L. A. G.: No-flow equilibrium and adsorption dynamics during ionic transport in soils, Nature, 283, 467–452, 1980.

Nash, J. E. and Sutcliffe, J. V.: River flow forecasting through conceptual models Part I – A discussion of principles, J. Hydrol., 10, 282–290, 1970.

Nimmo, J. R. and Mello, K. A.: Centrifugal techniques for measuring saturated hydraulic conductivity, Water Resour. Res., 27, 1263–1269, 1991.

Orr, W. J. C. and Butler, J. A. V.: The rate of diffusion of deuterium hydroxide in water, J. Chem. Soc., 303, 1273–1277, 1935.

Reedy, O. C., Jardine, P. M., Wilson, G. V., and Selim, H. M.: Quantifying the diffusive mass transfer of nonreactive solutes in columns of fractured saprolite using flow interruption, Soil Sci. Soc. Am. J., 60, 1376–1384, 1996.

Shukla, M. K., Lal, R., Owens, L. B., and Unkefer, P.: Land use and management impacts on structure and infiltration characteristics of soils in the North Appalachian region of Ohio, Soil Sci., 168, 167–177, 2003.

Sundaram, B., Feitz, A., de Caritat, P., Plazinska, A., Brodie, R., Coram, J., and Ransley, T.: Groundwater Sampling and Analysis – A Field Guide, Record 2009/27 95, Geoscience Australia, Canberra, 2009.

Timms, W. and Hendry, M.: Long-term reactive solute transport in an aquitard using a centrifuge model, Ground Water, 46, 616–628, 2008.

Timms, W., Hendry, M. J., Muise, J., and Kerrich, R.: Coupling centrifuge modeling and laser ablation inductively coupled plasma mass spectrometry to determine contaminant retardation in clays, Environ. Sci. Technol., 43, 1153–1159, 2009.

Timms, W. A., Crane, R., Anderson, D. J., Bouzalakos, S., Whelan, M., McGeeney, D., Rahman, P. F., Guinea, A., and Acworth, R. I.: Vertical hydraulic conductivity of a clayey-silt aquitard: accelerated fluid flow in a centrifuge permeameter compared with in situ conditions, Hydrol. Earth Syst. Sci. Discuss., 11, 3155–3212, doi:10.5194/hessd-11-3155-2014, 2014.

Totsche, K. U., Jann, S., and Kogel-Knabner, I.: Release of polycyclic aromatic hydrocarbons, dissolved organic carbon, and suspended matter from disturbed NAPL-contaminated gravelly soil material, Vadose Zone J., 5, 469–479, 2006.

Wehrer, M. and Totsche, K. U.: Detection of non-equilibrium contaminant release in soil columns: delineation of experimental conditions by numerical simulations, J. Plant Nutr. Soil Sc., 116, 475–483, 2003.

Wehrer, M. and Totsche, K. U.: Determination of effective release rates of polycyclic aromatic hydrocarbons and dissolved organic carbon by column outflow experiments, Eur. J. Soil Sci., 56, 803–813, 2005.

Wehrer, M. and Totsche, K. U.: Difference in PAH release processes from tar-oil contaminated soil materials with similar contamination history, Chem. Erde-Geochem., 69, 109–124, 2009.

Wilson, J. L. and Gelhar, L. W.: Analysis of longitudinal dispersion in unsaturated flow 1. The analytical method, Water Resour. Res., 17, 122–130, 1981.

Table 1. Core and influent properties, experimental parameters and K_v results for the interrupted-flow experiments. Calculations are based on Eq. (2) for K_v, Eq. (3) for estimated in situ total stress and Eq. (4) for total stress at the base of core specimen during centrifugation.

Core depth (m BGL)	Estimated in situ total stress, σ_i (kPa)	Influent groundwater depth (m BGL)	Influent EC ($\mu S\,cm^{-1}$)	g level applied	Core length, L_c (mm)	Height of influent water above core, h_c (mm)	K_v ($m\,s^{-1}$)	Total stress at base of core during centrifugation, σ_g (kPa)
5.03	89	10	18 470	20	36	61	1.4×10^{-8}	75
9.52	177	10	18 470	20	47	81	3.9×10^{-9}	127
21.75	383	20	13 160	80	54	48	5.1×10^{-9}	373

Table 2. Constrained ($D, L_c, \varnothing, \mu$) and unconstrained ($\varnothing_m$, α and γ) model parameters. a is calculated using Eq. (10).

Core depth (m BGL)	Core diameter, D (mm)	Core length, L (mm)	Total porosity, $\varnothing$	Pore volume of the mobile domain per total core volume, $\varnothing_m$	Coefficient of molecular diffusion, μ [$L^2\,T^{-1}$]	Hydro-dynamic dispersivity, α [L]	Mass transfer coefficient, γ [T^{-1}]	Half width of the matrix block, a (mm)
5.03	100	36	0.44	0.06	3.43×10^{-5}	$L_c/2$	0.65	18.3
9.52	100	47	0.47	0.04	3.43×10^{-5}	$L_c/2$	1.50	12.1
21.75	100	55	0.43	0.08	3.43×10^{-5}	$L_c/2$	1.20	12.3

Table 3. NSMEC for the core sample taken from 5.03 m depth BGL due to changes in constrained (L, $\varnothing$, μ) and unconstrained ($\varnothing_m$, α and γ) model parameters. Changes in constrained parameters comprised the estimated percentage error per each parameter, which was 2.78, 2.79 and 50 % for L, $\varnothing$ and μ respectively. Changes in unconstrained parameters were ±50 %. The NSMEC for the best fit was 0.972.

Model Parameter	Pore volume of the mobile domain per total pore volume, $\varnothing_m$	Mass transfer coefficient, γ	Hydrodynamic dispersivity, α	Total porosity, $\varnothing$	Core length, L	Coefficient of molecular diffusion, μ
NSMEC (+change)	0.925	0.926	0.952	0.974	0.965	0.964
NSMEC (−change)	0.952	0.862	0.964	0.968	0.971	0.975
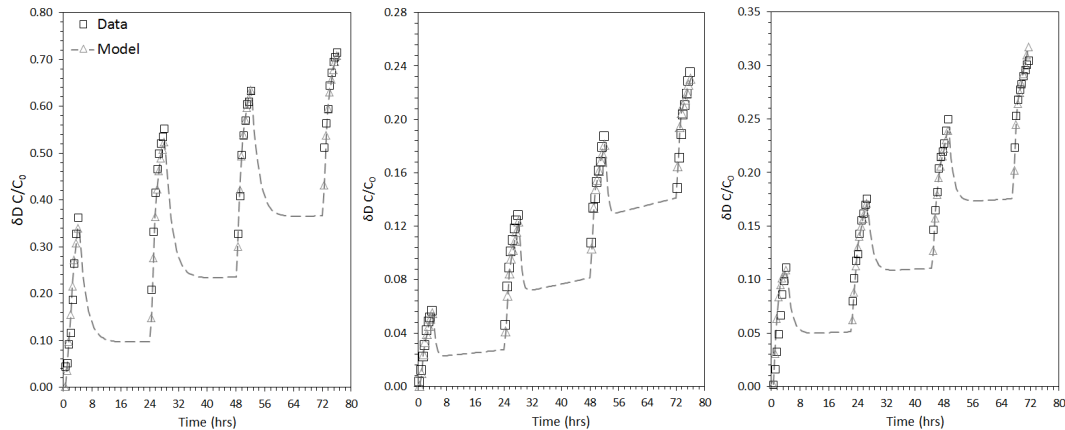
Figure 1. Normalised D_2O breakthrough data along with best fit dual porosity model output for the interrupted-flow experiments conducted using core samples taken from 5.03 m (left panel), 9.52 m (middle panel) and 21.75 m (right panel) depth BGL.
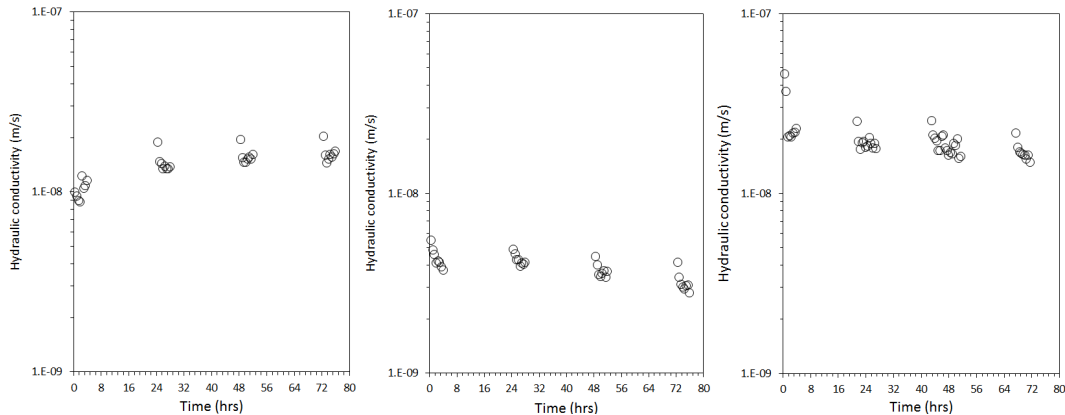
Figure 2. Vertical hydraulic conductivity ($\mathrm{m\,s^{-1}}$), calculated using Eq. (2), for the interrupted-flow experiments conducted using core samples taken from 5.03 m (left panel), 9.52 m (middle panel) and 21.75 m (right panel) depth BGL.
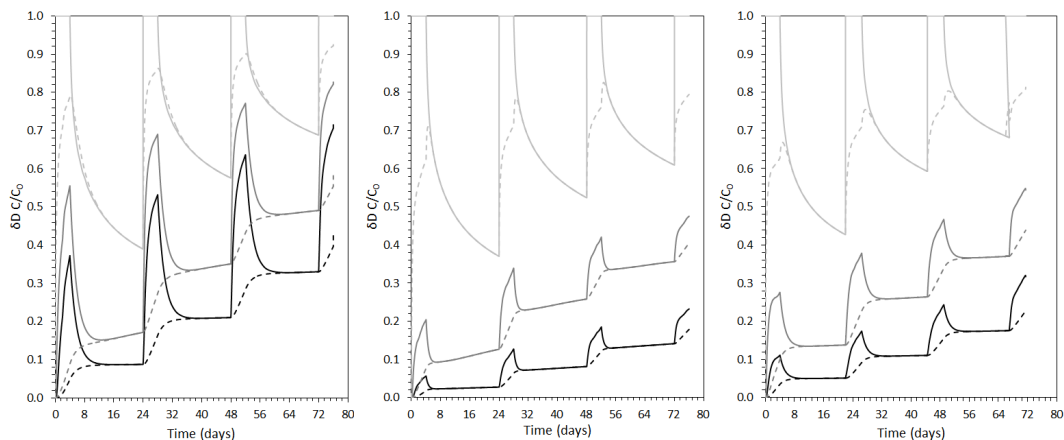
Figure 3. Model output for mobile (solid lines) and immobile (dashed lines) domains for core samples taken from 5.03 m (left panel), 9.52 m (middle panel) and 21.75 m (right panel) depth BGL. The black, dark grey and light grey lines comprise model output for the base, middle and top of the cores respectively.
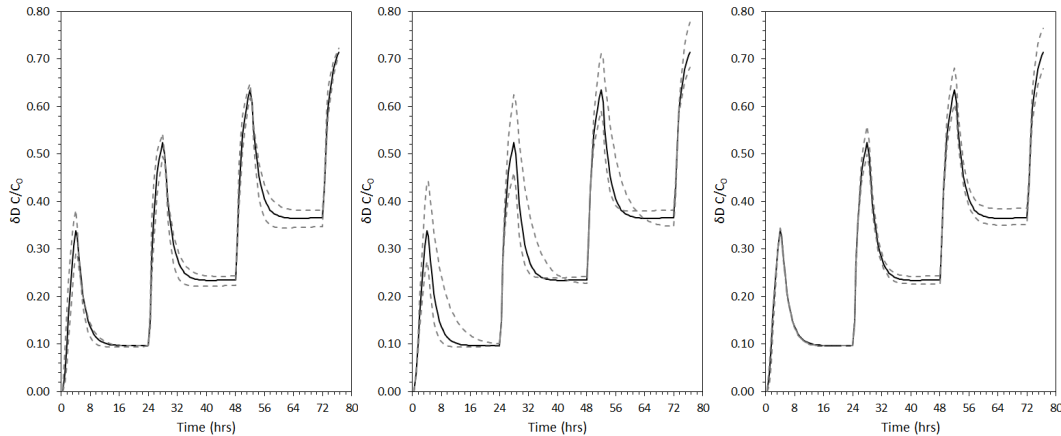
Figure 4. Sensitivity of the dual domain model for the core sample taken from 5.03 m depth BGL due to ±50 % change in unconstrained parameters: $\varnothing_m$ (LHS), γ (middle) and α (RHS).
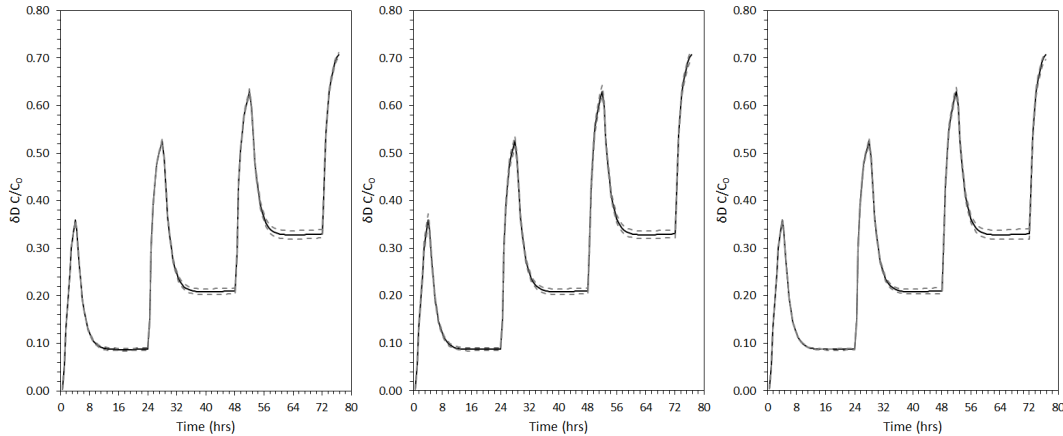
Figure 5. Sensitivity of the dual domain model for the core sample taken from 5.03 m depth BGL for the calculated error associated with the constrained parameters: ⌀ (LHS); L (middle) and μ (RHS).